

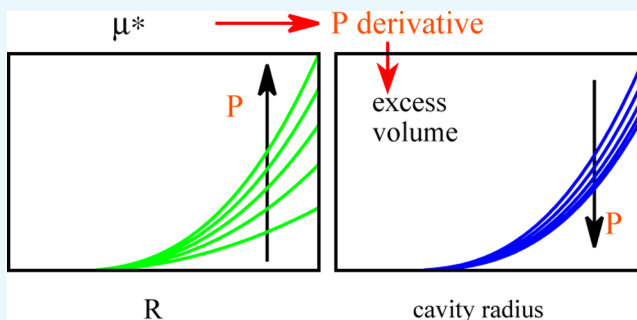
Excess Volumes from the Pressure Derivative of the Excess Chemical Potential: Testing Simple Models for Cavity Formation in Water

Franca Maria Floris*

Dipartimento di Chimica e Chimica Industriale, Università di Pisa, Via Giuseppe Moruzzi 13, 56124 Pisa, Italy

S Supporting Information

ABSTRACT: Excess volumes and excess compressibilities for hard spheres in water were computed by pressure derivatives of the excess chemical potential, which is equivalent to the work of cavity formation. This is relevant to the application of continuum solvation methods at various pressures. The excess chemical potential was modeled within phenomenological expressions for curved surfaces plus a pressure–volume term, for which two approaches were adopted, differing for the radius of the spherical volume. This implies a different dependence on pressure of parameters. In all cases, in the surface term, for the pressure derivative of parameters of the curvature function, use was made of the previously proposed expressions for the first two moments obtained from the density and radial distribution of oxygens in liquid water. Only for the parameter which has the dimension of surface tension (γ) was explicit dependence on pressure considered and results are affected by the specific polynomial used. In agreement with what inferred from simulation results obtained for cavities in TIP4P water, negative and positive adsorptions at the contact radius were extrapolated for a very large cavity at 1 and 8000 atm, respectively. The expressions here employed for the excess chemical potential predict the zero value of asymptotic adsorption to be at a pressure between 500 and 800 atm, which can be compared to results from the revised scaled particle theory. In the same range, for a nanometer-sized cavity, a change of behavior occurs regarding the ratio between the excess Helmholtz free energy and the product between pressure and excess volume.



INTRODUCTION

Partial molar volumes and related quantities, such as excess volumes and excess compressibility, are relevant to the study of the pressure effect on the variation of free energy in processes occurring in solutions,^{1–10} mixtures,^{11,12} and complex environments.^{13–19} The study of molecular hydration and molecular interactions in water under increasing pressure is essential to any full discussion of the pressure denaturation of proteins,^{2,7,17,18} which has stimulated many of these works. On this important problem of molecular biology, there have been various significant contributions since Kauzmann in 1959²⁰ suggested that the hydrophobic effect should have a prominent role in the stability of the folded form of a protein.

In the end of the 1990s, pressure dependence of hydrophobic interactions was studied by Hummer et al.¹⁰ and water incorporation into the protein was indicated as the dominant effect that accompanies the unfolding of a protein upon increasing pressure. More recently, on the basis of a detailed study of a methane-like solute in water up to 3000 atm,⁷ it has been concluded that the change in volume related to the exposure of a small hydrophobic solute is negative when comparing high pressure to atmospheric pressure, which appears to be consistent with what is expected in the unfolding of a protein.

However, this consistency cannot give a complete explanation of the problem, and for some authors,^{17,18} the hydrophobic effect is inadequate or irrelevant, whereas the change in volume associated with the exposure of hydrophilic groups is much more important. In their investigation on the origins of pressure denaturation of a protein, Chalikian and MacGregor¹⁸ found that solvation of peptide groups is a major driving force in the process, whereas that of polar side chains should not be so important. According to the same authors, another major driving force is the “the presence and partial disappearance of large intraglobular voids”, which still in some way leads back to hydrophobicity. This aspect has been discussed also by Rouget et al.²¹ and Roche et al.²² Although this is only a brief survey of the main ideas on the issue, it is sufficient to illustrate the great complexity of the problem, which is still open to debate. Indeed, the origin of the volume decrease associated with the unfolding of a protein has not yet been completely understood, even if it has been recognized that changes in the solvent distribution can have an important role in determining the sign of this volume change.^{7,17,21}

Received: August 9, 2017

Accepted: September 22, 2017

Published: October 5, 2017

Thus, the accurate computation of excess volumes appears to be very important. Simulations can be very useful to obtain insights into this field,^{7–9,13–16,18,19} provided very long runs can be carried out to reduce uncertainty. This explains why only in the past two decades the use of simulations to compute volumetric quantities has increased,^{5–9,13–16,18,19,23–25} thanks to more powerful computing resources. A comparison of different methods used to compute excess volumes has shown consistency in their results,^{7,9,23,25} which are generally in good agreement with experimental data.^{5–7,9,24} Because radial distribution functions are commonly obtained from simulations and statistical theories, the first widely used method was that based on Kirkwood–Buff (KB) integrals.²⁶ Problems related to the statistical ensemble can be managed, and this method is useful for the interpretation of the results.^{5,12,14,23,25} However, the so-called direct method^{7,9,23,25} is important because, without using further elaboration, it simply applies the definition of partial molar volume working in the isobaric isothermal ensemble.^{2,4} Within a third possible method, excess volumes are computed from the slope of the curve that fits the variation of free energy as a function of pressure when T is held constant.^{7–9} This method has been applied to realistic models of solutes in water and other solvents, with the variation of free energy computed by either the perturbative method or thermodynamic integration.⁹

Similar studies could be carried out with continuum solvation models,²⁷ although these have so far been applied mainly at atmospheric pressure. Within these models, a very accurate quantum mechanical^{28,29} description of the solute is possible, and this can provide new insight into the pressure effect on solvation and interactions, especially when the dissolved molecule contains hydrophilic groups. On the other hand, there is the challenge of a reasonable parameterization of these models to not miss important effects. Indeed, the free energy is computed as sums of terms and a crucial point is the calculation of the change of free energy associated with the formation of the cavity,^{27,30} to which this study is devoted.

In these calculations, the cavity is of suitable size and its shape is modeled on the solute geometry. However, for the aim of this study, it is convenient to consider the simplest case of a spherical cavity because there is the advantage of using simple expressions,^{30–32} from which pressure derivatives are easily obtained³³ to compute excess volumes. The pitfalls of the approximate model based on the scaled particle theory (SPT) in computing excess volumes at low²³ and high pressures are well known,²⁵ whereas the revised theory (RSPT) seems to provide satisfactory results.^{34,35} Alternative models^{30–32} formulated within the thermodynamics of surfaces have not yet been tested on volumetric quantities.

For a macroscopic cavity, all of the models mentioned above have the same radial scaling. Thus, a general model includes a pressure–volume term and a surface term, which is the product of a constant ($\tilde{\gamma}$), the area of the surface, and a curvature factor. It is the specific function used for this factor that determines the accuracy of calculations and differences between models. The aim of this study is to show that by adding a few terms to the curvature factor of the well-known Tolman expression³⁶ it is possible to obtain acceptable values of excess volumes for cavities in water.

At fixed pressure and temperature, these models describe how the variation of free energy depends on the cavity radius, which defines a spherical exclusion region for the centers of water molecules.^{23,25,33} There are no limitations in the possible

cavity size studied, whose cavity radius might be seen as the contact radius with the center of a hypothetical solute. For this reason, the same terminology formulated within the thermodynamics of solutions is maintained,^{2,4} and the change of free energy associated with the formation of the cavity is equivalent to the excess chemical potential^{2,8} or pseudochemical potential (μ^*) of a hard-sphere solute.

Models were tested by comparison with the simulation results of cavities in contact with water oxygens. It is this contact distance, here called cavity radius, that defines the studied system, whereas the other measure of the cavity size^{27,30,37} is the radius of the empty region, or “void”,²⁵ that is, the region excluded to “any part” of the solvent molecule. The radius of the void is defined as the difference between the contact distance (R) and the assumed value for water radius (r_w), typically in the range of 1.4–1.6 Å. However, the reader should keep in mind that the water molecule is nonspherical and that in real systems solute and solvent domains are not sharply separated because there is a region of electronic overlap.³⁸ Furthermore, the models discussed here are not suitable for cavities in which both oxygens and hydrogens have been excluded from the same region.³⁰ Indeed, the change of free energy associated with the formation of such a cavity is higher than that found when the check is made only on oxygen centers. Also the cavity–solvent radial distribution was found, in this case, to be very different.³⁰

Parameterization of μ^* at any pressure along the water isotherm at 298 K was explored in a previous work³³ for the commonly adopted division of the excess chemical potential, that is, using the accessible surface and the exclusion volume. The expression was tested on the contact value of the cavity–solvent radial distribution, which is related to the derivative of μ^* with respect to the cavity radius.

In the present work, examination of the derivative of μ^* with respect to pressure is done by comparison with simulation results of excess volumes obtained by the direct method.^{23,25} The investigation is also extended to a second approach, which refers to a modified pressure–volume term, in which the radius of the spherical volume is smaller than that of the cavity. In this way, the assumed volume includes additional terms in line with “border thickness” models.^{24,39–41} This might be a reasonable first approximation because more flexible expressions are necessary to fit simulation results of cavity excess volumes.^{4,23,25,42–44} However, these were found to be in between the volume of the void associated with the cavity and the exclusion volume, both used as reference volumes in the decomposition of excess volumes.²⁵ Within the second approach, some few cases were examined, with the assumed volume in this range. The expression is written in a general form and includes as a particular case that of the first approach, which is kept distinct from the second approach because the exclusion volume is the most natural choice as reference volume for cavities in a solvent.

The difference between the excess volume and the exclusion volume has a clear interpretation as the change in volume associated with cavity–solvent correlations,^{23,25} on which increasing pressure has a striking effect.³³ Simulation results^{23,25}

have shown that this change of volume can be positive or negative depending on the pressure and cavity radius. Thus, within the first approach, this means that the pressure derivative of the surface term in μ^* can be also negative, which at first sight can be difficult to explain. However, this is understandable if one recognizes the arbitrariness of the pressure–volume term

and that this is inevitable when modeling μ^* with the aim of obtaining excess volumes. Indeed, the two terms in the model do not correspond to those in the thermodynamic decomposition of μ^* , which can only be performed if the excess volume is known. Within the second approach, especially with an assumed volume close to that of the void associated with the cavity, the pressure derivative of the surface term may always result positive, which appears more in line with what is expected. It is shown that this is reflected in a positive derivative of parameter $\tilde{\gamma}$ with respect to pressure, whereas this derivative becomes negative at high pressures if the exclusion volume is assumed to be in the pressure–volume term. At the same time, curvature parameters are strongly affected. Relations between parameters in the two approaches are clearly defined as a function of pressure and can be used to check the scheme adopted in the parameterization, which for parameters entering the curvature factor uses implicit dependence through water density, described as a function of pressure with the expression proposed in a previous work. Nevertheless, these relations contain $\tilde{\gamma}$, for which a polynomial dependence on pressure is considered. Some focus is on volume-derived quantities, such as adsorption at the accessible surface and excess compressibility. Both quantities are relevant in the validation of expressions used to compute the excess chemical potential. In particular, asymptotic adsorption for a cavity of infinite radius is related to $\left(\frac{\partial \tilde{\gamma}}{\partial P}\right)_T$, as suggested by Ashbaugh et al.^{8,35} It is shown that the relation depends on the assumed pressure–volume term, whereas quantities that entail the thermodynamic decomposition of μ^* are not affected by the assumption made in the model.

METHODS

Excess Volumes from the Pressure Derivative of μ^* .

Starting from a pressure study at constant T of the excess chemical potential, μ^* , which defines the change of Gibbs free energy due to the addition of one solute molecule at a fixed position in the system,^{8,33,45} the excess volume can be obtained from the pressure derivative

$$v_s^* = \left(\frac{\partial \mu^*}{\partial P} \right)_T \quad (1)$$

From the second derivative, one can obtain the excess isothermal compressibility

$$\Delta K_T = - \left(\frac{\partial v_s^*}{\partial P} \right)_T \quad (2)$$

which differs from the partial molar isothermal compressibility only for contributions of solute translation.^{7,18,25} As commonly used, in the definition above, the capital letter refers to an apparent compressibility.¹⁸ The lowercase letter is used in the “excess compressibility” of Matubayasi and Levy⁵ (Δk_T), which corresponds to the product of the number density of the pure solvent and ΔK_T . In this work, excess quantities are defined with respect to an ideal solution, in which all molecular interactions are turned off,^{2,4} that is, the ideal gas. Thus, v_s^* is related to the partial molar volume, v_s , namely

$$v_s^* = v_s - k_T^0 k_B T \quad (3)$$

where k_T^0 is the solvent isothermal compressibility, k_B is the Boltzmann constant, and T is the temperature, and in

accordance with the thermodynamic definition, v_s , the partial molar volume is

$$v_s = \left(\frac{\partial V}{\partial N_s} \right)_{P,T,N_w} \quad (4)$$

with N_s and N_w being the numbers of solute and solvent molecules, respectively. In this work, an infinitely dilute solution is considered ($N_w \gg N_s$) so that solute–solvent interactions can be neglected. According to the definition given by eq 3, μ^* coincides with the pseudochemical potential defined by Ben-Naim,² and can be decomposed at constant pressure as

$$\mu^* = a^* + P v_s^* \quad (5)$$

where a^* is the excess Helmholtz free energy.^{4,45} In the case of a hard-sphere solute–solvent potential, at constant T , μ^* represents the reversible work necessary to form a cavity in the solvent,⁴⁶ and for very small cavities, it can be computed from a general equation⁴⁶ written in terms of the first two moments of solvent distribution.^{31–33,47} When water is the solvent, this is applicable to a cavity with radius less than ~ 1.85 Å. These radii are inappropriate to insert a real solute, but the study of such small cavities enables a parameterization at any pressure along the isotherm of a simple model used for larger cavities.³³ For this, the most common division^{8,33,45} of the excess chemical potential related to a cavity of radius R can be adopted

$$\mu^* = 4\pi \tilde{\gamma} f_c(R) R^2 + P \left(\frac{4\pi}{3} R^3 \right) \quad (6)$$

where $\tilde{\gamma}$ has the dimension of a surface tension and $f_c(R)$ is defined in terms of a length parameter $\tilde{\delta}^a$, an energy parameter w_0 , and a volume parameter α ^{32,33}

$$f_c(R) = 1 - \frac{\tilde{\delta}}{R} + \frac{w_0}{4\pi \tilde{\gamma} R^2} - \frac{\alpha}{R^3} \quad (7)$$

This function equals 1 for a cavity in the limit of infinite radius and includes standard curvature corrections up to the third power of $1/R$.^{31,32,48} As in SPT, the volume in eq 6 is named exclusion volume, which here represents the volume of the spherical region from which the entry of water oxygen centers was prevented in simulations.^{23,25} The corresponding surface of radius R defines the accessible surface, which is the most natural reference surface for the system.

A discussion on the meaning of parameters is beyond the scope of this study. Therefore, the surface term is not rewritten with respect to the equimolar surface,^{36,42–44} whose distance from the surface of tension defines the Tolman length.³⁶ This matter generally poses some difficult questions that would require specific analysis.^{32,49} Furthermore, the equimolar dividing surface can be defined only once the excess volume has been computed.^{42–44}

Pressure–Volume Term. The pressure–volume term in eq 6 represents the expansive work required to form the cavity in an ideal gas.⁴⁵ Actually, this term is different from that in eq 5 because the excess volume includes a nonideal contribution,^{5,23} which comes from molecular interactions and is here denoted by ΔV_{AIC}

$$v_s^* = \frac{4\pi}{3} R^3 + \Delta V_{AIC} \quad (8)$$

The acronym AIC stands for “all interactions coupled”, and in the specific systems studied in this work, we are referring to the coupling of water–water interactions after a spherical exclusion volume of radius R has been defined.^{23,25} The decomposition above can be derived from the KB integral.²⁶ Thus, ΔV_{AIC} arises from the difference between the real and ideal cavity–solvent correlation functions in the domain accessible to the center of the solvent. The ideal reference is that of a cavity in an ideal gas,⁵⁰ for which the cavity–solvent correlation is described by a Heaviside step function. In such a case, ΔV_{AIC} equals 0 and ν_s^* coincides with the exclusion volume defined by the cavity. At 298 K, the striking pressure effect on cavity–water radial distributions (rdf) was observed to be reflected in a very different behavior of $\Delta V_{\text{AIC}}(R)$.^{25,33}

At a constant pressure, a simple model is able to describe how ΔV_{AIC} varies with the increase of the cavity radius R .^{25,42–44} In particular, extrapolating to a nanometric radius, it was found reasonable to use the following simple description

$$\nu_s^* = \frac{4\pi}{3}R^3 + c_2R^2 + c_1R + c_0 \quad (9)$$

Thus, a comparable performance is in principle provided by the pressure derivative of eq 6, as it contains terms of the same power in R plus the additional term arising from α/R^3 in the curvature factor. Namely, this will depend on the range of R in which the equation is applied.

Concerning the interpretation of the surface term in eq 6, it is evident that its derivative with respect to pressure gives ΔV_{AIC} (see eq 8). Simulation results have shown that this quantity can be also negative, which is well explained in terms of cavity–water correlations. However, this implies that the surface term in μ^* can decrease under increasing pressure, which may seem unexpected if one does not recognize that the thermodynamic decomposition in eq 5 does not correspond to that in eq 6. However, this is inevitable if the excess volume is unknown and one wants to estimate its value from the pressure derivative of μ^* . In other words, this indicates that, when modeling the excess chemical potential, there is some arbitrariness in the pressure–volume term. Keeping its simplicity, eq 6 can be rewritten in a more general form

$$\mu^* = 4\pi\tilde{f}_c(R)R^2 + P\left(\frac{4\pi}{3}(R + \delta_R)^3\right) \quad (10)$$

where the pressure–volume term reduces to that of the more commonly used decomposition for the length parameter $\delta_R = 0$. With a negative value of δ_R , there is the possibility of having a surface term that increases with increasing pressure also when ΔV_{AIC} is negative. It is also worthwhile to note that the volume in eq 10 becomes the volume of the void associated with the cavity for $\delta_R = -r_w$, where r_w is the radius of a water molecule. The equation above preserves the asymptotic behavior of eq 6 for an infinite cavity radius. For instance, the value at contact of the cavity–solvent rdf, $G(R)$,⁴⁶ converges to $P/(\rho K_B T)$ with both equations. Furthermore, by writing R as a sum of contact radii, the volume in eq 10 is equivalent to that of the model initially proposed by Edward et al.⁵¹ and more recently employed in the analysis of simulation and experimental results.^{24,25,39–41,52}

Below, we refer to eqs 6 and 10, respectively, as the pressure cavity excluded volume (PCEV) and modified $P\Delta V$ (mPV) approaches. Differences in the results are expected to be within uncertainties that mainly derive from the number and quality of

data used in the parameterization. Indeed, the length δ_R does not increase the flexibility of the model but only changes the decomposition of μ^* , so determining different parameter values. Relations between parameters in the two approaches are clearly defined as a function of pressure as follows

$$\tilde{\gamma}_{\text{mPV}} = (\tilde{\gamma})_{\text{PCEV}} - \delta_R P \quad (11)$$

$$\tilde{\delta}_{\text{mPV}} = \frac{(\tilde{\gamma}\tilde{\delta})_{\text{PCEV}} + \delta_R^2 P}{(\tilde{\gamma})_{\text{PCEV}} - \delta_R P} \quad (12)$$

$$(w_0)_{\text{mPV}} = (w_0)_{\text{PCEV}} - \frac{4\pi}{3}\delta_R^3 P \quad (13)$$

$$\alpha_{\text{mPV}} = \frac{(\tilde{\gamma}\alpha)_{\text{PCEV}}}{(\tilde{\gamma})_{\text{PCEV}} - \delta_R P} \quad (14)$$

The relations above can be used to check the scheme adopted in the parameterization, which for parameters entering the curvature factor uses implicit dependence through density. Nevertheless, these relations contain $\tilde{\gamma}$, for which a polynomial dependence on pressure is considered, regardless of the approach (PCEV or mPV). Henceforth, to avoid the complicated notation above, the same symbols are used for the parameters independently of the approach, which is defined by the fixed value of δ_R .

Adsorption at the Accessible Surface and $\tilde{\gamma}(P)$. At the accessible surface, which is defined by the cavity radius R , the excess number of solvent molecules is related to ΔV_{AIC} ^{42–44}

$$n_s(R) = -\rho\Delta V_{\text{AIC}} \quad (15)$$

where ρ is the solvent number density. From this quantity, the solvent adsorption at the same reference surface is readily obtained

$$\Gamma(R) = \frac{n_s(R)}{4\pi R^2} \quad (16)$$

This is an absolute adsorption that strongly depends on the position of the reference or dividing surface, which in this case coincides with the cavity surface.^{42,43} Thus, in the expression above, the notation is simplified with respect to the more general one used in refs 42, 43. Originally, this quantity was used within the thermodynamics of interfaces in the Gibbs approach,³⁶ which was then extended to boundary surfaces.⁵³ Here, an excess number of molecules still arises from the discrepancy between the real solvent distribution around the hard-sphere solute with respect to an “ideal” distribution defined by the position of the dividing surface, that is, a Heaviside function. Following Ashbaugh and Truskett,⁸ the sign of the asymptotic value of Γ in the limit of a large cavity radius determines if $\tilde{\gamma}$ increases or decreases with increasing pressure. This suggestion is based on the comparison of the pressure derivative of μ^* (eq 6) with the decomposition made in eq 8.

Thus, under conditions near to saturation, because of desorption at the accessible reference surface for a large cavity of infinite radius,^{8,23,42–44,54} a positive slope of $\tilde{\gamma}$ against pressure should be expected. Moving away from these conditions, at higher values of P along the isotherm, the opposite should occur on the basis of a study of hydrophobic solutes.⁵⁵ This is also in line with the different behavior shown at 1⁴² and 8000 atm³³ when increasing the cavity radius. All said, the above holds for the PCEV approach (eq 6);³³

Table 1. Effect of the Assumed Pressure–Volume Term in μ^* on the Parameterization along the Isotherm at 298 K^a

model	δ_R^b (Å)	$\tilde{\gamma}$	α	$w_0/(4\pi\tilde{\gamma})^c$	$\tilde{\delta}^d$
PCEV	0.00	[21, 82]	[1.43, 13]	[3.45, 24.91]	[3.0, 16]
mPV_A	−0.50	[63, 93]	[1.43, 3.3]	[3.45, 7.62]	[3.0, 4.5]
mPV_B1	−1.00	[81, 122]	[1.43, 2.23]	[3.45, 4.73]	[3.0, 3.5]
mPV_B2	−1.00	[79.2, 116]	0.99 ^e	[3.45, 4.73]	[2.8, 3.0]
mPV_C	−1.38	[81, 161]	[1.43, 1.8]	[3.45, 4.10]	[3.0, 3.2]
mPV_D	−1.75	[81, 198]	[1.43, 1.6]	[3.45, 3.88]	[3.0, 3.3]

^aFor PCEV (eq 6) and mPV (eq 10) models, which are characterized by a different value of δ_R , the extremes of values of parameters $\tilde{\gamma}$ (dyn/cm), α (Å³), $w_0/(4\pi\tilde{\gamma})$ (Å²), and $\tilde{\delta}$ (Å) are reported. ^bFor an assumed value of water radius, r_w , the border thickness is obtainable from $\delta_R + r_w$.²⁵ ^cNote that $G(R)$ does not depend on w_0 , which is a constant term in μ^* . ^dHere and in ref 33 $\tilde{\delta}$ stands for twice the parameter defined with the same symbol in ref 32 where W denotes a quantity that is equivalent to μ^* . ^e α was fixed along the isotherm at the optimal value from the least-squares fit of $d\mu^*/dR$ at 1 atm.³²

however, when using the mPV approach (eq 10), the pressure derivative of $\tilde{\gamma}(P)$ is accordingly modified

$$\left(\frac{\partial \tilde{\gamma}}{\partial P}\right)_T = -\frac{\Gamma_\infty}{\rho} - \delta_R \quad (17)$$

where Γ_∞ is the asymptotic value of adsorption at infinity (i.e., for a very large cavity radius). In this way, for δ_R held constant, $\tilde{\gamma}$ has a corresponding contribution proportional to pressure. This is in agreement with eq 11.

RESULTS AND DISCUSSION

Parameterization of μ^* and Prediction of $G(R)$.

By computing $\left(\frac{\partial \mu^*}{\partial R}\right)_{P,T}$, the average density of solvent centers at the cavity surface, $\rho G(R)$,^{31,46} can be obtained and $G(R)$ can be compared to simulation results of the cavity–water oxygen pair correlation.^{32,33} An efficient parameterization procedure of eq 6 was proposed and discussed in detail in a previous work.³³ Briefly, its main features are: (1) it is alternative to fitting but less expensive; (2) it requires a preliminary study at several pressures to determine $\tilde{\gamma}(P)$; (3) for a fixed value of $\tilde{\gamma}$, the other parameters, α , $\tilde{\delta}$, and w_0 , are determined from conditions on $G(R)$, $G'(R)$, and $\mu^*(R)$, applied at a chosen small radius (R_0). In the preliminary study (point (2)), operations described on point (3) were repeated at a fixed value of P until the optimal value of $\tilde{\gamma}$ was found so that simulation results of $G(R)$ for a sufficient large radius (R_1) were reproduced. In this way, data of $\tilde{\gamma}$ were determined along the isotherm with statistical uncertainties derived from those of $G(R_1)$. Regarding the third point, continuity conditions are imposed between eq 6 and μ^* written in terms of the first two moments of water distribution,^{31–33,46,47} from which follow conditions on the derived quantities, $G(R)$ and $G'(R)$. Owing to a complete description of the first two moments of water distribution as functions of R and P , the aforementioned conditions can be readily applied at any pressure along the isotherm. Within the limit of a small cavity so that no more than two solvents centers can be found in the spherical region of radius R , these quantities can be directly introduced into the general relation derived from statistical mechanics written for μ^* .⁴⁶

The same procedure was applied to eq 10 for some fixed negative values of δ_R (see Table 1). These appear reasonable on the basis of values found at 1 and 8000 atm²⁵ when fitting simulation results of excess volumes with the spherical volume of radius $R + \delta_R$, which is an extremely simple model equivalent to the so-called border thickness model.^{24,39–41,52} Parameters cover different ranges (Table 1), in agreement with eqs 11–14. In particular, for a negative δ_R , as shown in Figure 1, $\tilde{\gamma}$ of mPV

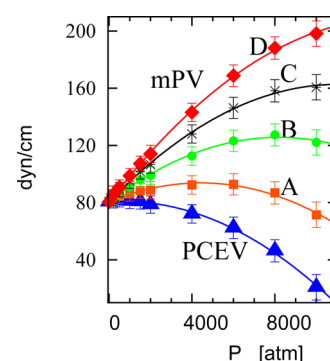


Figure 1. Pressure dependence at $T = 298$ K for parameter $\tilde{\gamma}$ (dyn/cm) obtained for different values of δ_R , which defines the pressure–volume term in μ^* (eqs 6 and 10). For PCEV, $\delta_R = 0$, whereas for cases A–D within mPV approach, see Table 1. Curves represent quadratic weighted least-squares fit.

models is larger than that of PCEV, and the difference increases linearly with an increasing of pressure ($\Delta\tilde{\gamma} = -\delta_R P$). A smaller range of values, for a more negative δ_R , is instead the main effect on the other parameters, which define the curvature function $f_c(R)$ (eq 7). As an example, the dependence on pressure of the length parameter $\tilde{\delta}$ is shown in Figure 2, where curves for mPV models were obtained from eq 12. Propagated errors from $G(R_1)$ were found to be smaller than those with the PCEV approach, especially for the case D and at pressures greater than 4000 atm.

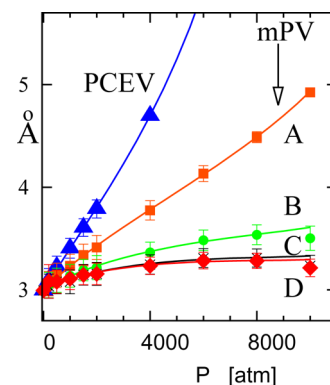


Figure 2. Pressure dependence at $T = 298$ K for parameter $\tilde{\delta}$ (Å) obtained for different values of δ_R (Table 1), which defines the pressure–volume term in μ^* (eqs 6 and 10). mPV curves for cases A (orange), B (green), C (black), and D (red) within mPV approach were obtained from PCEV curve (blue) using eq 12.

In spite of the striking effect on the parameters of the surface term, as expected, the same performance was found for the PCEV and mPV models. Here, their prediction capability on $G(R)$ is measured by comparison with simulation results.^{32,33} Indeed, it should be noted that only data corresponding to $R_1 = 6.05$ Å were used in the parameterization. In Table 2, the

Table 2. Comparison with NPT MC Simulation Results of $G(R)$ for Cavities in TIP4P Water^{56,a}

model	χ_1^b	χ_2^c	χ_3^d
PCEV and mPV	0.077	0.048	0.092
mPV_B2	0.059	0.146	0.100

^aPerformance of models measured as the square root of the average square deviation at fixed constant pressures of 1 atm (χ_1) and 8000 atm (χ_2) and along the water isotherm at 298 K for a cavity radius R of 2.85 Å. ^b $P = 1$ atm and R between 1.75 and 10 Å. ^c $P = 8000$ atm and R between 1.75 and 6.05 Å. ^d P between 1 and 10 000 atm and $R = 2.85$ Å.

square root of the average quadratic deviation is reported, regarding comparison of radial scaling at fixed pressures of 1 and 8000 atm and a comparison along the isotherm for a cavity radius of 2.85 Å.

At 8000 atm, comparison made for the PCEV approach was demonstrated to be very good³³ (Figure S2). This is also highlighted by the comparison at fixed R along the isotherm shown in Figure 3. At low pressure, and particularly at 1 atm,

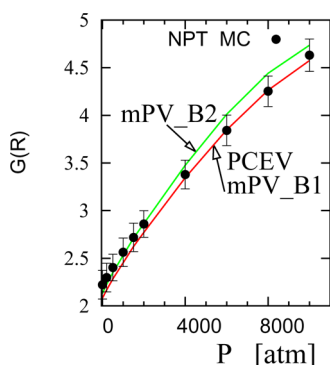


Figure 3. $G(R)$ values of cavity–water oxygen computed by NPT MC simulations of a cavity with $R = 2.85$ Å in 512 TIP4P waters at 298.15 K and several pressures along the isotherm (filled circles with error bars). Comparison with values predicted by simple models of μ^* , from which $G(R)$ was obtained by computing the derivative with respect to R .³³ Results practically do not depend on δ_R (Table 1), as shown in the figure for PCEV and mPV_B1 (red line), for which pressure dependence of parameter α was considered. The green line refers to MPV_B2 parameterization with α fixed at its optimal value at 1 atm.

models underestimate $G(R)$, whereas they give very good agreement with simulation results at a pressure greater than 3000 atm. At atmospheric pressure (Figure S1), the maximum value of $G(R)$ occurs for R very close to the value chosen for the comparison (2.85 Å).³² In this case, the largest discrepancy was observed relative to the range defined by the two radii that were used in the parameterization procedure ($R_0 = 1.67$ Å and $R_1 = 6.05$ Å). It is worthwhile emphasizing that underestimated values in this range are accompanied by overestimated values of $G(R)$ for a nanometer-sized cavity. However, for the examined cases, discrepancies were small and generally within statistical uncertainties, as shown in Figure 3.

At low pressure, less than 3000 atm, a better agreement with simulation results of $G(R)$ is obtained if α is assumed to be independent of P and fixed to the optimal value obtained by fitting results at 1 atm³² (Tables 1 and 2). In this case, continuity conditions were applied on μ^* and $G(R)$ but not on $G'(R)$. However, as shown in Figure 3, results at greater pressure are worse than those obtained when the normal procedure was used, regardless of the value of δ_R . This occurs also for $\delta_R = -1.75$ Å, for which α was found almost constant along the isotherm (Table 1).

Modeling $\tilde{\gamma}$ along the Isotherm and Computing Γ_∞

First and second derivatives with respect to P of all parameters entering eqs 6 and 10 were calculated from the assumed pressure dependence of $\tilde{\gamma}$ and the first two moments of water distribution.³³ Hence, excess volumes and derived quantities were computed. A crucial point of the procedure is an appropriate choice of the function $\tilde{\gamma}(P)$ because its derivative with respect to pressure is sensitive to the kind of description used. As shown in Figure 1, a quadratic function is generally sufficient to fit data in the whole range of pressure, even though results on quantities arising from $\left(\frac{\partial \tilde{\gamma}}{\partial P}\right)_T$ did not appear completely satisfactory, especially at low pressures. Therefore, polynomials of higher degree were investigated fitting $\tilde{\gamma}$ in some different ranges of pressure (Table 3).

The quantity here examined is Γ_∞ , which is directly obtainable from $\left(\frac{\partial \tilde{\gamma}}{\partial P}\right)_T$, water density, and δ_R (eq 17). These

Table 3. Adsorption Asymptotic Values (Γ_∞) in Å⁻² Obtained from eq 17 at Pressures of 1 and 8000 atm and the Computed Transition Pressure, $P_{-/+}$ (atm), from Negative to Positive values of Γ_∞ ^a

model for μ^*	$\tilde{\gamma}(P)$ fit (n)	P range (atm)	$P = 1$ atm		$P = 8000$ atm		$P_{-/+}$ (atm)
			$\left(\frac{\partial \tilde{\gamma}}{\partial P}\right)_T$	Γ_∞	$\left(\frac{\partial \tilde{\gamma}}{\partial P}\right)_T$	Γ_∞	
PCEV	2	10 000	0.09	-0.003	-0.98	0.040	669
	3	2000	0.4	-0.014			646
	3	4000	0.38	-0.013			676
	3	6000	0.20	-0.007			676
	3	8000	0.20	-0.004	-0.1	0.032	683
	4	4000	0.5	-0.015			613
	4	6000	0.4	-0.014			638
	4	8000	0.3	-0.010	-0.8	0.050	689
	5	6000	0.5	-0.016			596
	5	8000	0.46	-0.015	-1	0.030	617
mPV_D	2	10 000	1.8	-0.003	0.77	0.040	677
	3	2000	2.3	-0.018			599
	3	4000	2.2	-0.014			678
	3	6000	1.96	-0.007			742
	3	8000	1.87	-0.004	1	0.032	698
	4	4000	2.4	-0.022			549
	4	6000	2.2	-0.016			636
	4	8000	2.1	-0.010	1	0.051	696
	5	6000	2.5	-0.024			520
	5	8000	2.3	-0.018	1	0.024	610

^aResults from $\left(\frac{\partial \tilde{\gamma}}{\partial P}\right)_T$ (Å) and δ_R of PCEV and mPV_D models (see Table 1) are compared for different polynomial descriptions of $\tilde{\gamma}(P)$, whose degree (n) is indicated in the second column. Data of $\tilde{\gamma}$ derived from simulation results of $G(R)$ at various values of P for a cavity radius of 6.05 Å were fitted in various ranges of pressure, whose higher extreme is indicated in the third column.

values (Table 3) can be compared to those extrapolated at infinite radius from simulation results of $\Delta V_{\text{AIC}}(R)$ (eqs 8 and 15). By using for this purpose, a quadratic function (see eq 9), Γ_{∞} is -0.0394 \AA^{-2} at $P = 1 \text{ atm}$ ^{42–44} and 0.0331 \AA^{-2} at $P = 8000 \text{ atm}$.²⁵ The comparison shows that, at 8000 atm, a good agreement is found in some cases, whereas at 1 atm, there is generally some discrepancy, which is larger for the quadratic fit of $\tilde{\gamma}(P)$ along the isotherm. A less discrepant value from that extrapolated from eq 9 corresponds to fitting with cubic and fifth polynomials over a limited (2000–4000 atm) or a more extended range, respectively. Nevertheless, in agreement with what is expected, adsorption asymptotically converges to negative values at low pressures and to positive values at greater pressures. Transition between these opposite behaviors is illustrated in Figure 4 for the PCEV approach.

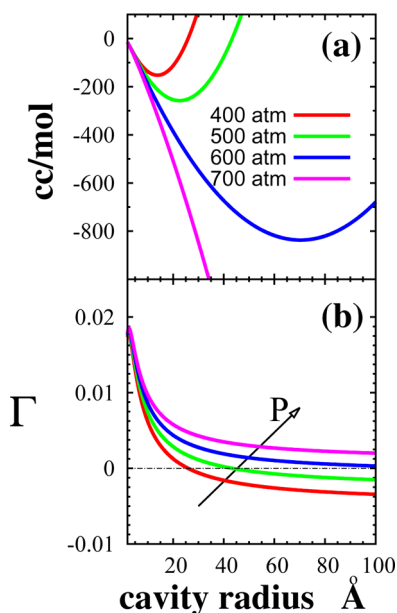


Figure 4. (a) Dependence on the cavity radius (R) of ΔV_{AIC} (eq 8) at pressures of 400, 500, 600, and 700 atm and temperature of 298.15 K. Results from PCEV approach (eqs 6 and 1) using for $\tilde{\gamma}(P)$ a cubic polynomial function fitted to data up to 2000 atm. (b) Adsorption Γ (Å⁻²) at the cavity surface obtained from ΔV_{AIC} for cases in (a) using eqs 15 and 16.

The pressure ($P_{-/+}$) at which Γ_{∞} changes sign from negative to positive falls in the range of 520–689 atm, the specific value being dependent on $\tilde{\gamma}(P)$ fit, as detailed in Table 3. However, as expected, results depend little on the model used for $\mu^*(R)$ and, for example, when $\tilde{\gamma}$ fitting is limited to data within 2000 atm, this pressure is estimated to be within 600–650 atm, regardless of the model assumed for μ^* . In some cases, by comparing mPV with PCEV results, discrepancies in $P_{-/+}$ can be larger than 50 atm. These are accompanied by differences in $\left(\frac{\partial \tilde{\gamma}}{\partial P}\right)_T$, showing that eq 17 is not exactly satisfied. This is a consequence of the fact that mPV data of $\tilde{\gamma}$ were not obtained from PCEV data (see eq 11) but simply by repeating the parameterization procedure with eq 10. Nonetheless, changes of 100 atm are possible even for a small change in R_0 , one of the two radii used in the parameterization. This happens, for instance, when comparing PCEV results of this work ($R_0 = 1.675 \text{ \AA}$) to those of the previous work³³ ($R_0 = 1.67 \text{ \AA}$), for

which $P_{-/+} = 784 \text{ atm}$ when using a quadratic function to fit $\tilde{\gamma}$ over 10 000 atm.

Radial Dependence of ν_s^* and ΔV_{AIC} at Constant Pressure: Comparison with Simulation Results. By varying the cavity radius, at 1 and 8000 atm, the PCEV and mPV approaches give similar results of excess volumetric quantities, even if the first performs slightly better. In the range delimited by the two radii used in the parameterization, Figure 5 depicts the best PCEV curves and simulation results of ν_s^*

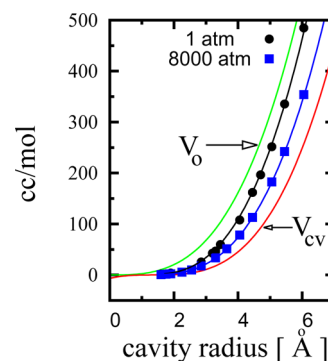


Figure 5. Dependence on the cavity radius (R) at 1 atm (black line) and 8000 atm (blue line) of the excess volume (ν_s^*) computed as the pressure derivative of μ^* at 298.15 K from eq 6 (PCEV approach) for $\tilde{\gamma}(P)$ described by a polynomial function of degrees 3 (1 atm) and 5 (8000 atm) fitting data up to 6000 atm (curve at 1 atm) and up to 8000 atm (curve at 8000 atm). Comparison with NPT MC results obtained by the direct method,^{23,25} at 1 atm (black filled circles) and at 8000 atm (blue filled squares). The green curve represents the excluded volume (V_0), whereas the red line is the volume of the cavity void (V_{cv}), that is, the spherical volume of radius $R - r_w$, for $r_w = 1.38 \text{ \AA}$.²⁵

obtained by the direct method. These PCEV results correspond to the $\tilde{\gamma}(P)$ for which the lowest average deviation was obtained. At the two pressures, this is measured by χ_4 and χ_5 (Table 4). By comparing the individual data values at atmospheric pressure, deviations are generally larger than three times the statistical uncertainties, but in the worst case ($R = 6.05 \text{ \AA}$), the relative error is less than 2%. Comparison is much better at 8000 atm, with agreement generally within two times the statistical uncertainties. Even at high pressure, the worst case is for the largest cavity and the relative error is less than 1%.

Simulation results at atmospheric pressure and at 8000 atm have shown a very different behavior when increasing the cavity radius.^{23,25} By considering the two references, that is, the exclusion volume and the cavity void (V_{cv}), ν_s^* is always in between for cavities with $R \leq 6.05 \text{ \AA}$ (Figure 5) at the two pressures considered. This should also characterize larger cavities at 8000 atm, as a consequence of the maintenance of structured hydrated shells.³³ On the contrary, at atmospheric pressure, when R is around 1 nm, due to the loss of structure that brings to dewetting at larger cavities, ν_s^* should become larger than the exclusion volume. Thus, this peculiarity is well analyzed in terms of ΔV_{AIC} (Figure 6), which becomes positive, so determining a negative adsorption (see eqs 15 and 16). This is consistent with the sign of Γ_{∞} discussed in the previous section.

The feature described above is found also in excess volumes computed as the pressure derivative of μ^* . However, the radius $R_{+/-}$ (Table 5) at which this change of behavior occurs depends

Table 4. Comparison with NPT MC Simulation Results of ν_s^* (cm³/mol): for Various $\tilde{\gamma}(P)$, the Performance of PCEV Model is Measured as the Square Root of the Average Square Deviation at Fixed Constant Pressures of 1 atm (χ_4) and 8000 atm (χ_5) and along the Water Isotherm at 298 K, for Cavity Radii R of 2.85 Å (χ_6) and 6.05 Å (χ_7)^a

$\tilde{\gamma}(P)$ fit	P range ^b	χ_4^c	χ_5^d	χ_6^e	χ_7^f
2	10 000	99.9 (6.6)	11.5	1.6	20.9
3	2000	41.5 (10)		2.2	12.1
3	4000	47.4 (8.6)		2.1	18.6
3	6000	79.7 (3.8)		1.7	9.2
3	8000	94.8 (5.7)	3.2	1.4	7.8
4	4000	34.9 (11.9)		2.1	10.3
4	6000	39.7 (10.5)		2.0	10.0
4	8000	63.5 (5.2)	21.5	1.9	18.3
5	6000	34.5 (10.5)		2.1	13.2
5	8000	35.4 (11.7)	1.0	1.9	10.5

^aIn the first column, the degree of the polynomial function used to describe the pressure dependence of parameter $\tilde{\gamma}$ is reported. ^bRange of pressure for the fitting of $\tilde{\gamma}$. ^c $P = 1$ atm and R between 1.75 and 10 Å. The value reported in the parenthesis refers to cavities with R between 1.75 and 6.05 Å. ^d $P = 8000$ atm and R between 1.75 and 6.05 Å. ^e P over the range used for the fitting and $R = 2.85$ Å. ^f P over the range used for the fitting and $R = 6.05$ Å.

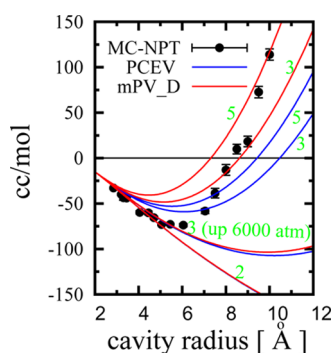


Figure 6. Dependence on the cavity radius (R) at 298.15 K and 1 atm of ΔV_{AIC} (eq 8) obtained from ν_s^* computed as the pressure derivative of μ^* , from eq 6 (PCEV approach) and eq 10 (mPV approach). For each model of μ^* , PCEV (blue lines) and mPV_D (red lines), the four curves refer to $\tilde{\gamma}(P)$ described by a polynomial function (see Table 3) fitting data in the pressure range of 1–2000 atm ($n = 3$), 6000 atm ($n = 3$ and 5), and 10 000 atm ($n = 2$). For the quadratic fit, PCEV and mPV_D lines practically overlap for the cavities shown in the figure. Black filled circles represent results from NPT MC simulations obtained from ν_s^* computed by the direct method.^{23,25}

on the pressure description adopted for $\tilde{\gamma}(P)$ (see Figure 6 and Table 3). For a quadratic polynomial fitting over the complete range of pressures investigated, this radius is overestimated with respect to simulation results, for which the inversion of sign was observed between 8 and 10 Å.^{23,25} By increasing the degree of the polynomial and decreasing the range of pressure of the fitted data, regardless of the value of δ_R in the expressions adopted for μ^* , it is possible to obtain improved results of $R_{+/-}$. Generally, a better agreement for this quantity corresponds to the cases with a more negative Γ_∞ (see Table 3), but unfortunately this does not imply a quantitative agreement of ΔV_{AIC} (Figure 6), at least when this quantity increases with R (Figure 6). Indeed, χ_4 is larger when all of the data are included in the analysis (Table 4). Nevertheless, for R larger than 6.05 Å, the corresponding relative error on ν_s^* is 4–5%. It is

Table 5. Cavity Radii $R_{+/-}$ (Å) at which $\Gamma(R)$ Becomes Negative when $P = 1$ atm and $T = 298$ K^a

$\tilde{\gamma}(P)$ fit (n)	P range (atm)	PCEV	mPV_D	mPV_B ₂
		$R_{+/-}$	$R_{+/-}$	$R_{+/-}$
2	10 000	38.0	37.6	^b
3	2000	10.5	8.6	10.1
3	4000	11.2	10.3	11.5
3	6000	18.7	18.1	37.6
3	8000	29.8	28.7	^b
4	4000	9.8	7.8	9.1
4	6000	10.3	9.3	10.0
4	8000	13.8	13.1	16.4
5	6000	9.4	7.3	8.7
5	8000	9.8	8.7	9.3

^aResults from pressure derivative of μ^* , modeled as in eq 6 (PCEV) or as in eq 10 (see Table 1) for different polynomial descriptions of $\tilde{\gamma}(P)$, whose degree is indicated in the first column. Parameters were determined by fitting data between 1 atm and the pressure indicated in the second column. Data of $\tilde{\gamma}$ derived from simulation results of contact values of $G(R)$ at various values of P for a cavity radius of 6.05 Å. ^b Γ_∞ was always positive.

worthwhile recalling that statistical uncertainties on $\tilde{\gamma}$ data were in all cases much more larger than discrepancies between the fitting curves, which mainly differ for the computed slope (Table 3). Therefore, the critical problem of having accurate derivatives is reflected in volume calculations based on the pressure derivative of μ^* . This suggests that the number of data should be increased and statistical uncertainties on $G(R)$ should be further reduced.

At the same time, the expression used for μ^* appears to be important. At a qualitative level, the simple models here investigated are able to predict the nonmonotonic behavior and the change of sign of ΔV_{AIC} . In this respect, they perform better than the approximate SPT expression^{23,33,46} but can likely be improved by adding some other term,⁴⁸ or modified to have a more accurate scaling from small to nanometer-sized cavities.^{8,32} Nevertheless, within the range of radii for which this volumetric quantity decreases (Figure 6), it is possible to achieve a satisfactory agreement with simulation results (Table 4). This happens also at a constant high pressure, 8000 atm (Figure 7), for which a good performance of the simple models here investigated is reasonably expected also at larger cavities because ΔV_{AIC} is predicted to vary monotonically with R , without change of sign.

Dependence on Pressure of ν_s^* at Fixed Radius: Comparison with Simulation Results.

In line with what is observed for small cavities (see Appendix), excess volumes of larger cavities mainly decrease when pressure increases with slopes that become more pronounced when cavity radius increases. In Figures 8 and 9, simulation results obtained by the direct method^{23,25} are shown for radii of 2.85 and 6.05 Å, respectively. These cavities can approximately hold, respectively, a water molecule and a hypothetical spherical solute slightly larger than the fullerene molecule. Curves in the figures refer to results obtained from pressure derivatives of μ^* described within the PCEV approach for some $\tilde{\gamma}(P)$ profiles. Results from the mPV approach were very similar (Figures S5–S8), in particular when the normal parameterization was used, that is, including the dependence on pressure of parameter α .

On average, for both cavities (see the last two columns of Table 4), the best description of dependence on pressure of ν_s^*

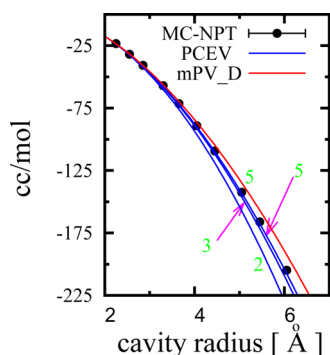


Figure 7. Dependence on the cavity radius (R) at 298.15 K and 8000 atm of ΔV_{AIC} (eq 8) obtained from ν_s^* computed as the pressure derivative of μ^* , from eq 6 (PCEV approach) and eq 10 (mPV approach). For each model of μ^* , PCEV (blue lines), and mPV_D (red lines), the curves refer to $\tilde{\gamma}(P)$ described by a polynomial function (see Table 3) fitting data in the pressure range of 1–8000 atm for $n = 2, 3, 5$ (green numbers). Lines practically overlap in all cases, except for $n = 5$. Black filled circles represent results from NPT MC simulations obtained from ν_s^* computed by the direct method.^{23,25}

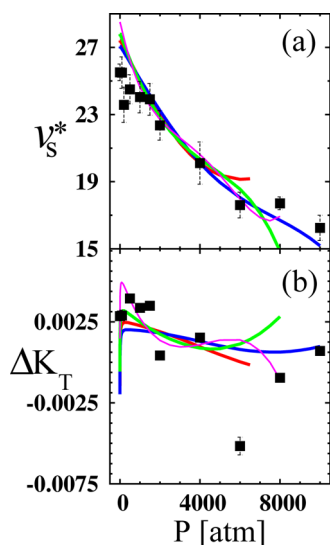


Figure 8. (a) Simulation results at 298.15 K of ν_s^* (cc/mol) computed by the direct method (points with error bars) for a cavity radius of 2.85 Å in TIP4P water plotted against pressure. Lines represent results from pressure derivative of μ^* computed within the PCEV approach (eq 6) for some $\tilde{\gamma}(P)$ profiles (see Table 3) and water density described with eq 7 of previous work.³³ The blue line corresponds to $\tilde{\gamma}$ fitted to data over 8000 atm with a cubic polynomial function. In the same range, $\tilde{\gamma}$ was fitted with polynomial functions of degree 4 (green line) and degree 5 (magenta line). The red line corresponds to the fit over 6000 atm with a cubic polynomial function. (b) The negative pressure derivative of ν_s^* (cc/(mol atm)) vs pressure obtained from simulation results of volumes and compressibility²⁵ (points with error bars). Lines obtained from the second derivative of μ^* within PCEV (colors as in (a)).

corresponds to a cubic polynomial fitting of $\tilde{\gamma}$ in the range of pressure up to 8000 atm. In this case, a good extrapolation at 10 000 atm was observed, whereas by extending the range, the results were worsened and very similar to those obtained by a quadratic profile of $\tilde{\gamma}(P)$ (Figure 10). Discrepancies with respect to simulation results were found within three times the statistical uncertainties for $R = 2.85$ Å, but become larger for $R = 6.05$ Å. However, these were more significant for the smaller

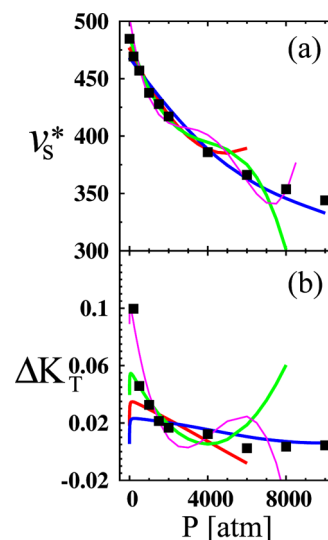


Figure 9. (a) Simulation results at 298.15 K of ν_s^* (cc/mol) computed by the direct method (points with error bars) for a cavity radius of 6.05 Å in TIP4P water plotted against pressure. Lines represent results from pressure derivative of μ^* computed within the PCEV approach (eq 6) for some $\tilde{\gamma}(P)$ profiles (see Table 3) and water density described with eq 7 of previous work.³³ The blue line corresponds to $\tilde{\gamma}$ fitted to data over 8000 atm with a cubic polynomial function. In the same range, $\tilde{\gamma}$ was fitted with polynomial functions of degree 4 (green line) and degree 5 (magenta line). The red line corresponds to the fit over 6000 atm with a cubic polynomial function. (b) The negative pressure derivative of ν_s^* (cc/(mol atm)) vs pressure obtained from simulation results of volumes and compressibility²⁵ (points with error bars). Lines obtained from the second derivative of μ^* within PCEV (colors as in (a)).

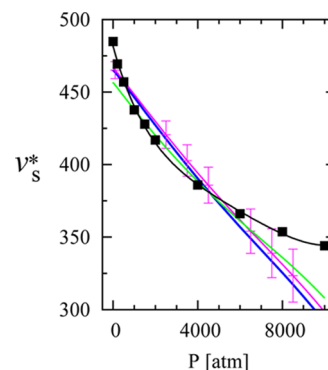


Figure 10. Simulation results at 298.15 K of ν_s^* (cc/mol) computed by the direct method (filled squares) for a cavity radius of 6.05 Å in TIP4P water plotted against pressure. The black line represents results from fits of quantities related to average accessible volumes in the solution and in water with eq 16 of previous work.²⁵ Colored lines represent results from pressure derivative of μ^* computed within the PCEV approach (eq 6) for a quadratic fit of $\tilde{\gamma}(P)$ made over 10 000 atm. The blue line (this work) differs from the red line³³ only for R_0 , the radius used in the parameterization. The error bars refer to evaluated propagated errors. The green line differs from the red line only for parameters in eq 16 of the previous work²⁵ fitted to experimental data of water density instead of TIP4P water (see ref 33).

cavity, with a relative maximum error of 13%, whereas for the larger cavity, this was of 3%. As shown in Figures 8 and 9, a better agreement is reached over a range up to 4000 atm by increasing the degree of the polynomial or decreasing the range of pressure in the fitting of $\tilde{\gamma}$ (see also Table 4). This happens

in particular for the larger cavity, with relative discrepancies generally within 1%. Correspondingly, it is evident that there is an improvement in the slope when compared to the simulation results of ΔK_T (Figures 8b and 9b).

Sensitivity to density was studied within the same approach for μ^* and using the two expressions proposed in a previous work³³ for the pressure dependence of water density with optimal parameters determined by fitting experimental or TIP4P data. It can be noted that these different data give the same trend with pressure, with excess volumes generally in good agreement, the discrepancies being within or only slightly larger than three times the errors estimated from parameters' uncertainties. For clarity, in Figure 10, comparison only with results relative to the PCEV approach is shown. The same conclusions on sensitivity to density were reached with the modified $P\Delta V$ (mPV) approach and regardless of the model adopted for $\tilde{\gamma}(P)$.

Excess Helmholtz Free Energy from the Thermodynamic Decomposition of μ^* . Using the thermodynamic decomposition of μ^* (eq 5), which holds for the cavity formation at constant pressure, the excess Helmholtz free energy, a^* , was computed as the difference between μ^* and $P\nu_s^*$ for excess volumes computed from the pressure derivative of μ^* . The asymptotic value for a cavity of infinite radius of the corresponding excess Helmholtz free energy per unit area, $a^*/(4\pi R^2)$, is plotted against pressure in Figure 11. Results depend

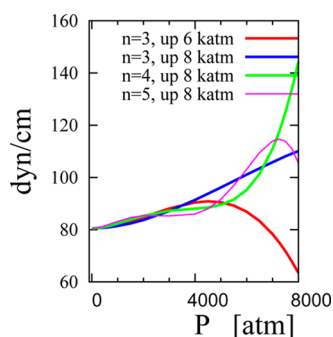


Figure 11. Asymptotic value ($R \rightarrow \infty$) of the excess Helmholtz free energy per unit area, $a^*/(4\pi R^2)$, plotted against pressure at 298.15 K. Results obtained from μ^* and ν_s^* (eq 5) using PCEV approach for some $\tilde{\gamma}(P)$ profiles (see Table 3) and TIP4P water density described with eq 7 of previous work.³³

on the $\tilde{\gamma}(P)$ description and can be characterized by a plateau between 2000 and 4000 atm or increase monotonically with increasing pressure, as in the case of the cubic polynomial fitting data up to 8000 atm. The presence of a maximum is unexpected and should indicate wrong extrapolation or an artifact due to fitting conditions. Nevertheless, in all cases, values fall in the same range spanned by the parameter $\tilde{\gamma}$, and are in between those of the PCEV and mPV_C models (Figure 1). However, these parameters have no particular meaning and can be very different (Figure 1), but this does not affect significantly the derived thermodynamic quantities. Indeed, as for excess volumes, the two approaches investigated yield very similar results (Figure S9).

Thus, also the ratio $P\nu_s^*/a^*$ was found to be weakly dependent on the pressure–volume term assumed in the model. Figure 12 shows the striking effect of increasing pressure for cavities with R within 10 nm. Under ambient conditions, in agreement with general solvation processes,^{2,4}

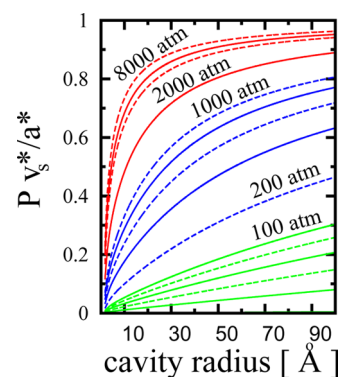


Figure 12. Effect of increasing pressure on the ratio $P\nu_s^*/a^*$ plotted against the cavity radius R at 298.15 K. Results obtained from the PCEV approach and a fifth polynomial to fit $\tilde{\gamma}(P)$. Green lines refer to pressures up to 100 atm (increments of 20 atm), blue lines refer to pressures between 200 and 1000 atm (increments of 100 atm), and red lines refer to pressures between 2000 and 8000 atm (increments of 2000 atm).

$P\nu_s^*$ is very small with respect to a^* . Far from these conditions, the weight of $P\nu_s^*$ increases, becoming dominant at very high pressures. For a cavity of 10 nm, the relative importance of the two contributions to μ^* is inverted approximately at the pressure at which Γ_∞ becomes positive (see $P_{-/+}$ in Table 3). On the other hand, for a cavity of 1 nm, this occurs at a higher pressure (~ 2000 atm).

Optimal Value of δ_R and the Border Thickness. The spherical volume in eq 10 can be used to fit data of excess volumes:

$$\nu_s^* = \frac{4\pi}{3}(R + \delta_R)^3 \quad (18)$$

and it is equivalent to the so-called border thickness model, which has been used to fit experimental data of various molecules in water, including some proteins.^{24,40} The border thickness is recovered from $\delta_R + r_w$ for an assumed value of r_w , the radius of a water molecule. For $r_w = 1.38$ Å, the border thickness of cavities in TIP4P water falls in the range of 0.72–1.38 Å at atmospheric pressure for R up to 1 nm, whereas at 8000 atm, its value drops to ≈ 0.5 Å.²⁵ The results at 1 atm reflect dewetting at the cavity–water interface²⁵ and are consistent with those found for soft spherical repulsive solutes.⁴¹ Attractive solute–water interactions bring about a smaller border thickness,⁴¹ and its value increases from 0.4 to 1 Å, for “cavity volumes” extracted from experimental data of solutes with van der Waals radii between 3 and 7 Å.⁴⁰ According to Ashbaugh et al.,⁴¹ this is related to the assumed spherical shape of the solute and the “molecular border thickness”, with values within 0.5 Å, increases very little with solute size. The “spherical border thickness” model, albeit approximate, remains useful for correlating partial molar volumes and making comparisons. However, one should be aware that it is a phenomenological expression and it should be interpreted with some caution. In particular, given the definition of an exclusion volume in the systems studied in this work, the border thickness cannot be assimilated to the thickness of an “empty layer devoid of water surrounding the solute”.²⁵

Differently from when fitting excess volumes, as stated in previous sections, δ_R cannot be considered a “true” parameter in the expression of the excess chemical potential defined by eq

10 because it does not add flexibility to the model. Therefore, there is no interest to optimize its value to improve results of excess volumes obtained by the pressure derivative of μ^* . Nevertheless, an appropriate choice of its value can be based on other considerations. For instance, with a negative value of δ_R around -1.75 Å, the surface term increases with increasing pressure and curvature parameters show small variations along the isotherm compared to those of the PCEV approach ($\delta_R = 0$). Furthermore, eq 11 suggests the possibility of deriving a comparable length quantity from the asymptotic value of the excess Helmholtz free energy per unit area

$$\delta_\infty^* = \lim_{R \rightarrow \infty} \frac{\frac{a^*}{4\pi R^2} - (\tilde{\gamma})_{\text{PCEV}}}{P} \quad (19)$$

This quantity is plotted in Figure 13a, and the corresponding border thickness in Figure 13b. Results obtained with different

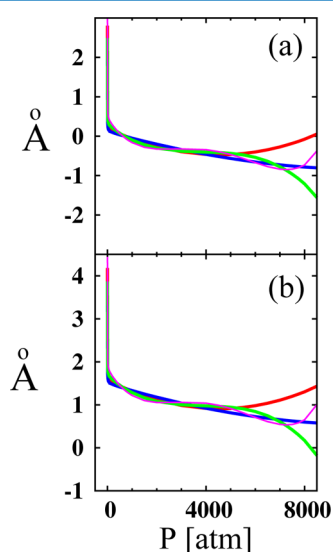


Figure 13. (a) Pressure dependence at 298.15 K for the length δ^* (Å) obtained from eq 19 with a^* derived from μ^* and ν_s^* within PCEV approach in the asymptotic limit for a cavity of infinite radius. Lines represent results for some $\tilde{\gamma}(P)$ profiles (see Table 3) and TIP4P water density described with eq 7 of previous work.³³ The blue line corresponds to $\tilde{\gamma}$ fitted to data over 8000 atm with a cubic polynomial function. In the same range, $\tilde{\gamma}$ was fitted with polynomial functions of degree 4 (green line) and degree 5 (magenta line). The red line corresponds to the fit over 6000 atm with a cubic polynomial function. (b) The corresponding border thickness computed as $\delta^* + r_w$ (colors as in (a)).

values of $\tilde{\gamma}(P)$ substantially agree up to 4000 atm, where the decrease seen at low pressures could be related to the decrease in dewetting at the cavity–water interface expected under increasing pressure. The large value of 3–4 Å could be consistent with the increase of the border thickness with cavity size, which was observed at 1 atm, whereas the value at 8000 atm is very close, in one case, to that found fitting simulation results. This happens for $\tilde{\gamma}(P)$ described by a cubic polynomial and fitted up to this pressure. On the basis of the above, it seems quite reasonable to introduce as δ_R in eq 18 the function $\delta^*(R, P)$ defined in eq 19. Hence, with this model for excess volumes, the pressure of zero adsorption at the accessible surface ($P_{-/+}$) is obtained for $\delta_\infty^* = 0$, which corresponds to a border thickness of 1.38 Å (see Figure 13). Its value falls in the

range of 700–800 atm, which is higher by 50–100 atm than the values reported in Table 3.

CONCLUSIONS

Regardless of the approach, the results of Γ_∞ computed by the simple models investigated were consistent with the sign of adsorption values extrapolated at infinity from simulation results at 1 and 8000 atm, these being negative and positive, respectively. This change of behavior is here predicted to occur between 500 and 800 atm. However, when considering the cases for which a more negative Γ_∞ is obtained at atmospheric pressure, this range decreases to 600–650 atm. This pressure also marks the crossover from $a^* > P\nu_s^*$ to $a^* < P\nu_s^*$ regimes for a cavity of ~ 10 nm.

PCEV and mPV approaches yield similar results of excess volumes and are qualitatively in agreement with simulation results. At a quantitative level, relative errors generally were within a few percentages. It is worthwhile remarking that results obtained from the method based on the pressure derivatives of μ^* are very sensitive to $\left(\frac{\partial \tilde{\gamma}}{\partial P}\right)_T$. In fact, within the same approach, for a variety of polynomial description of $\tilde{\gamma}(P)$, some disagreement is possible on volumetric quantities despite a good agreement on $G(R)$ and μ^* . On the other hand, pressure dependence of water density and of the average number of oxygen pairs observed in spherical region of radius less than 1.85 Å are fundamental in determining the main qualitative features of pressure dependence of ν_s^* and compressibility.

Clearly, the simple models investigated in the present work are much more valid at greater pressure than at low pressure, for which more sophisticated expressions are necessary. Further improvement can be expected from a more accurate description of the excess chemical potential in scaling from microscopic to nanometric cavity size,^{32,34,35} as well as using additional information in the parameterization. On the basis of comparison at atmospheric pressure with expressions formulated in the framework of the thermodynamics of surfaces³² and over the range of 3000 atm with revised scaled particle theory (RSPT),^{34,35} values of $\tilde{\gamma}$ obtained with simple models appear overestimated by approximately 10–15 dyn/cm. At the same time, $P_{-/+}$ appears underestimated by about 200–400 atm.

SIMULATION DETAILS

Simulation results used for comparisons in this work have been published and discussed in previous works.^{23,25,32,33,43,44} NPT Monte Carlo simulations at 298.15 K were run using a version of the BOSS⁵⁷ program, which was appropriately modified to study hard-sphere cavities in water. For water molecules, the TIP4P potential⁵⁶ was used. At atmospheric pressure, $N_w = 216$, 512, and 1435 for cavity radii up to 10 Å, whereas for the other pressures, $N_w = 512$ for cavity radii up to 6.05 Å. In all cases, the center of the cavity was fixed at the center of the box and water–water interactions were truncated with a cutoff of $L/2$ (L being the box length). Very long simulations were run to reduce statistical uncertainties in excess volumes, which were computed by the direct method. The number of MC configurations used to compute averages varied between 5×10^8 and 5×10^{10} .

APPENDIX A

For $R \leq 1.85$ Å, excess volumes can be obtained from the pressure derivative of μ^* , written in terms of the first two

moments of pure water due to the heuristic model describing their dependence on radius and pressure.^{33,46} Volumetric quantities obtained with this method are important because all of these basic relations were used in the parameterization and application of eqs 6 and 10. At a fixed cavity radius, excess volume dependence on P is shown in Figure 14a, where

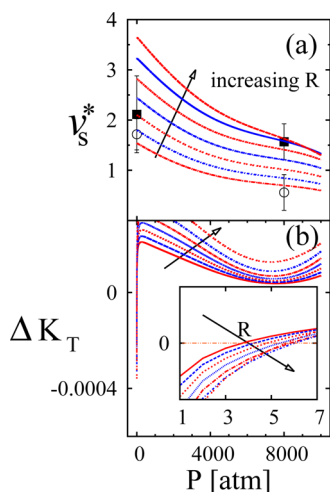


Figure 14. Small cavities in TIP4P water at $T = 298$ K (R between 1.60 and 1.90 Å, step of 0.5 Å). (a) Pressure dependence of ν_s^* (cm³/mol) obtained from P derivative of μ^* written in terms of the first two moments of water distribution (see eqs 7, 9 and 10 of a previous work³³). Values from MC simulations of cavities in TIP4P water are also shown for radii of 1.60 Å (circles) and 1.75 Å (filled squares) at 1 and 8000 atm. (b) Pressure dependence of the corresponding negative pressure derivative (eq 2). The inset shows the same quantity in the range of -0.0002 to 0.0002 cm³/(mol atm) for P between 1 and 7 atm. Arrows indicate increasing R .

comparison is made with simulation results obtained by the direct method for some selected radii at pressure values of 1 and 8000 atm. Results are in agreement within statistical uncertainties. Unfortunately, these were quite significant, despite simulation runs being very long. This is a well-known limitation of the direct method when it is applied to such small cavities.^{8,23,43,44}

As shown in the figure, excess volumes generally decrease with pressure. For such small cavities, it can be supposed that this mainly depends on the decrease in water compressibility. The excess isothermal compressibility, ΔK_T , computed as the negative pressure derivative of ν_s^* , is shown in Figure 14b. Even if this quantity is very small, the observed trend with increasing pressure is interesting because of some similarities with results obtained for methane in water.⁷ The inset in the figure shows that at low pressures excess compressibility changes sign from negative to positive at a value of P that increases with cavity radius. For the largest cavities in the range, this occurs at a pressure of ≈ 6 atm. Namely, the comparison above can hold only at a qualitative level, and a systematic comparison with simulation results of ΔK_T for such small cavities is beyond of the scope of this work. We simply report that at 8000 atm negative values were obtained in disagreement with the positive (even if very small) values shown in Figure 14b. Discrepancies are larger than statistical uncertainties and could be ascribed to systematic errors in volumes or to some limitations of the theory.^{58,59}

■ ASSOCIATED CONTENT

Supporting Information

The Supporting Information is available free of charge on the ACS Publications website at DOI: 10.1021/acsomega.7b01157.

Comparison of $G(R)$ with simulation results; excess volumes and excess compressibility for the mPV_D and mPV_B₂ approaches (PDF)

■ AUTHOR INFORMATION

Corresponding Author

*E-mail: floris@dcci.unipi.it.

Notes

The author declares no competing financial interest.

■ ACKNOWLEDGMENTS

The author thanks the University of Pisa for financial support under the project PRA_2016_46 "Study of confined systems: towards a multi-scale approach".

■ ADDITIONAL NOTE

^aBy definition, $\tilde{\delta}$ stands for twice the parameter defined with the same symbol in ref 32 where the symbol W was used for the work of cavity formation, which is equivalent to the pseudochemical potential μ^* .^{33,46}

■ REFERENCES

- (1) Cabani, S.; Gianni, P.; Mollica, V.; Lepori, L. Group Contribution to the Thermodynamic Properties of Non-Ionic Organic Solutes in Dilute Aqueous Solution. *J. Solution Chem.* **1981**, *10*, 563–595.
- (2) Ben-Naim, A. *Statistical Thermodynamics for Chemists and Biochemists*; Plenum: New York, 1992.
- (3) Ben-Amotz, D. Chemical Reaction Volumes in Model Fluid Systems. 1. Hard-Sphere Solvation and Diatomic Dissociation Precesses. *J. Phys. Chem.* **1993**, *97*, 2314–2319.
- (4) Ben-Amotz, D.; Raineri, F. O.; Stell, G. Solvation Thermodynamics: Theory and Applications. *J. Phys. Chem. B* **2005**, *109*, 6866–6878.
- (5) Matubayasi, N.; Levy, R. M. Thermodynamics of the Hydration Shell. 2. Excess Volume and Compressibility of a Hydrophobic Solute. *J. Phys. Chem. B* **1996**, *100*, 2681–2688.
- (6) Lockwood, D. M.; Rossky, P. J. Evaluation of Functional Group Contributions to Excess Volumetric Properties of Solvated Molecules. *J. Phys. Chem. B* **1999**, *103*, 1982–1990.
- (7) Moghaddam, M. S.; Chan, H. S. Pressure and Temperature Dependence of Hydrophobic Hydration: Volumetric, Compressibility, and Thermodynamic Signatures. *J. Chem. Phys.* **2007**, *126*, 114507–114522.
- (8) Ashbaugh, H. S.; Truskett, T. M. Putting the squeeze on cavities in liquids: Quantifying pressure effects on solvation using simulations and scaled-particle theory. *J. Chem. Phys.* **2011**, *134*, 014507–014517.
- (9) Vilseck, J. Z.; Tirado-Rives, J.; Jorgensen, W. Determination of partial molar volumes from free perturbation theory. *Phys. Chem. Chem. Phys.* **2015**, *17*, 8407–8415.
- (10) Hummer, G.; Garde, S.; Garcia, A. E.; Pohorille, A.; Pratt, L. R. The pressure dependence of hydrophobic interactions is consistent with the observed pressure denaturation of proteins. *Proc. Natl. Acad. Sci. U.S.A.* **1998**, *95*, 1552–1555.
- (11) Matteoli, E.; Mansoori, G. A., Eds. *Advances in Thermodynamics Fluctuation Theory of Mixtures*; Taylor & Francis: New York, 1990; Vol. 2.
- (12) Chitra, R.; Smith, P. E. Properties of 2,2,2-trifluoroethanol and water mixtures. *J. Chem. Phys.* **2001**, *114*, 426–435.
- (13) Baynes, B. M.; Trout, B. L. Proteins in Mixed Solvents: A Molecular-Level Perspective. *J. Phys. Chem. B* **2003**, *107*, 14058–14067.

- (14) Smith, P. E. Cosolvent Interactions with Biomolecules: Relating Computer Simulation Data to Experimental Thermodynamic Data. *J. Phys. Chem. B* **2004**, *108*, 18716–18724.
- (15) Kang, M.; Smith, P. E. Preferential Interaction Parameters in Biological Systems by Kirkwood-Buff Theory and Computer Simulation. *Fluid Phase Equilib.* **2007**, *256*, 14–19.
- (16) Priya, M. H.; Ashbaugh, H. S.; Paulatis, M. E. Cosolvent Preferential Molecular Interactions in Aqueous Solutions. *J. Phys. Chem. B* **2011**, *115*, 13633–13642.
- (17) Ben-Naim, A. Theoretical Aspects of Pressure and Solute Denaturation of Proteins: A Kirkwood-Buff-Theory Approach. *J. Chem. Phys.* **2012**, *137*, 235102–235110.
- (18) Chalikian, T. V.; Macgregor, R. B., Jr. Origins of Pressure-Induced Protein Transitions. *J. Mol. Biol.* **2009**, *394*, 834–842.
- (19) Meng, B.; Ashbaugh, H. S. Effect of hydrostatic pressure on gas solubilization in micelles. *Langmuir* **2015**, *31*, 3318–3325.
- (20) Kauzmann, W. *Adv. Protein Chem.* **1959**, *14*, 1.
- (21) Rouget, J. B.; Aksel, T.; Roche, J.; Saldana, J. L.; Garcia, A. E.; Barrick, D.; Royer, C. A. Size and sequence and the volume change of protein folding. *J. Am. Chem. Soc.* **2011**, *133*, 6020–6027.
- (22) Roche, J.; Caro, J. A.; Norberto, D. R.; Barthe, P.; Roumestand, C.; Schlessman, J. L.; Garcia, A. E.; Moreno, B. G.; Royer, C. A. Cavities determine the pressure unfolding of proteins. *Proc. Natl. Acad. Sci. U.S.A.* **2012**, *109*, 6945–6950.
- (23) Floris, F. M. Nonideal Effects on the Excess Volume from Small to Large Cavities in TIP4P Water. *J. Phys. Chem. B* **2004**, *108*, 16244–16249.
- (24) Patel, N.; Dubins, D. N.; Pomes, R.; Chalikian, T. V. Parsing Partial Molar Volumes of Small Molecules: A Molecular Dynamics Study. *J. Phys. Chem. B* **2011**, *115*, 4856–4862.
- (25) Floris, F. M. Effect of increasing pressure on excess volume for cavities in TIP4P water. *J. Mol. Liq.* **2016**, *222*, 38–46.
- (26) Kirkwood, J.; Buff, F. The Statistical Mechanical Theory Of Solutions. *J. Chem. Phys.* **1951**, *19*, 774–777.
- (27) Tomasi, J.; Mennucci, B.; Cammi, R. Quantum Mechanical Continuum Solvation Models. *Chem. Rev.* **2005**, *105*, 2999–3093.
- (28) Amovilli, C.; Filippi, C.; Floris, F. M. Quantum Monte Carlo formulation of volume polarization in dielectric continuum theory. *J. Chem. Phys.* **2008**, *129*, 244106–244112.
- (29) Amovilli, C.; Floris, F. M. Study of dispersion forces with Quantum Monte Carlo: Toward a Continuum Model for Solvation. *J. Phys. Chem. A* **2015**, *119*, 5327–5334.
- (30) Floris, F.; Selmi, M.; Tani, A.; Tomasi, J. Free Energy and Entropy for Inserting Cavities in Water: Comparison of Monte Carlo Simulation and Scaled Particle Theory Results. *J. Chem. Phys.* **1997**, *107*, 6353–6365.
- (31) Pratt, L.; Pohorille, A. Theory of hydrophobicity: Transient cavities in molecular liquids. *Proc. Natl. Acad. Sci. U.S.A.* **1992**, *89*, 2995–2999.
- (32) Floris, F. M. Modeling the Cavitation Free Energy. *J. Phys. Chem. B* **2005**, *109*, 24061–24070.
- (33) Floris, F. M. The formation of a cavity in water: changes of water distribution and prediction of the excess chemical potential of a hard-sphere solute under increasing pressure. *J. Mol. Liq.* **2016**, *218*, 166–173.
- (34) Ashbaugh, H. S.; Pratt, L. Scaled-Particle Theory and the Length Scales of Hydrophobicity. *Rev. Mod. Phys.* **2006**, *78*, 159–178.
- (35) Ashbaugh, H. S.; da Silva Moura, N.; Houser, H.; Wang, Y.; Goodson, A.; Barnett, J. W. Temperature and pressure dependence of the interfacial free energy against a hard surface in contact with water and decane. *J. Chem. Phys.* **2016**, *145*, No. 124710.
- (36) Rowlinson, J.; Widom, B. *Molecular Theory of Capillarity*; Clarendon Press: Oxford, 1951.
- (37) Graziano, G. Scaled Particle Theory of the Length Scale Dependence of Cavity Thermodynamics in Different Liquids. *J. Phys. Chem. B* **2006**, *110*, 11421–11426.
- (38) Amovilli, C.; Filippi, C.; Floris, F. M. Coupling Quantum Monte Carlo to a nonlinear continuum model for spherical solutes. *J. Phys. Chem. B* **2006**, *110*, 26225–26231.
- (39) Chalikian, T. V.; Totrov, M.; Abagyan, R.; Bresauler, K. J. The Hydration of Globular Proteins as Derived from Volume and Compressibility Measurements: Cross Correlating Thermodynamic and Structural Data. *J. Mol. Biol.* **1996**, *260*, 588–603.
- (40) Patel, N.; Dubins, D. N.; Pomes, R.; Chalikian, T. V. Size dependence of cavity volume: A molecular dynamics study. *Biophys. Chem.* **2012**, *161*, 46–49.
- (41) Ashbaugh, H. S.; Barnett, J. W.; da Silva Moura, N.; Houser, H. E. Hydrated nonpolar solute volumes: Interplay between size, attractiveness, and molecular structure. *Biophys. Chem.* **2016**, *213*, 1–5.
- (42) Floris, F. M. Excess Densities and Equimolar Surfaces for Spherical Cavities in Water. *J. Chem. Phys.* **2007**, *126*, 074505–074513.
- (43) Floris, F. M. Note: Volumes Errors and Equimolar Surfaces. *J. Chem. Phys.* **2012**, *136*, 116102–116103.
- (44) Floris, F. M. Erratum: “Note: Volume errors and equimolar surfaces” [*J. Chem. Phys.* *136*, 116102 (2012)]. *J. Chem. Phys.* **2013**, *138*, No. 059901.
- (45) Stillinger, F. H. Structure in Aqueous Solutions of Nonpolar Solutes from the Standpoint of Scaled-Particle Theory. *J. Solution Chem.* **1973**, *2*, 141–158.
- (46) Reiss, H.; Frish, H.; Lebowitz, J. Statistical Mechanics of Rigid Spheres. *J. Chem. Phys.* **1959**, *31*, 369–380.
- (47) Hummer, G.; Garde, S.; Garcia, A. E.; Pohorille, A.; Pratt, L. R. An information theory model of hydrophobic interactions. *Proc. Natl. Acad. Sci. U.S.A.* **1996**, *93*, 8951–8955.
- (48) Siderius, D. W.; Corti, D. S. On the Use of Multiple Interpolation Functions in Scaled Particle Theory to Improve the Predictions of the Properties of the Hard-Sphere Fluid. *J. Chem. Phys.* **2007**, *127*, 144502–144521.
- (49) Hill, T. J. *Phys. Chem.* **1952**, *56*, 526–531.
- (50) Barrat, J. L.; Hansen, J. P. *Basic Concepts for Simple and Complex Liquids*; Cambridge University Press: Cambridge, U.K., 2003.
- (51) Edward, J. T.; Farrel, P. G. Relation between van der Waals and Partial molal volumes of Organic Molecules in water. *Can. J. Chem.* **1975**, *53*, 2965–2970.
- (52) Graziano, G. On the magnitude of border thickness in the partial molar volume of cavities in water. *Chem. Phys. Lett.* **2013**, *570*, 46–49.
- (53) Viece, J. J.; Reiss, H. Thermodynamics of Curved Boundary Layers. *J. Chem. Phys.* **1972**, *57*, 3745–3753.
- (54) Mittal, J.; Hummer, G. Static and Dynamic Correlations in Water at Hydrophobic Interfaces. *Proc. Natl. Acad. Sci. U.S.A.* **2008**, *105*, 20130–20135.
- (55) Sarupria, S.; Garde, S. Quantifying Water Density Fluctuations and Compressibility of Hydration Shells of Hydrophobic Solutes and Proteins. *Phys. Rev. Lett.* **2009**, *103*, 037803–037807.
- (56) Jorgensen, W.; Chandrasekhar, J.; Madura, J.; Impey, R.; Klein, M. Comparison of Simple Potential Functions for Simulating Liquid Water. *J. Chem. Phys.* **1983**, *79*, 926.
- (57) Jorgensen, W. BOSS, version 3.5; Yale University Press: New Haven, CT, 1994.
- (58) Hummer, G.; Garde, S.; Garcia, A. E.; Pratt, L. R. New Perspectives on Hydrophobic Effects. *Chem. Phys.* **2000**, *258*, 349–370.
- (59) Southall, N. T.; Dill, K. A.; Haymet, D. J. A View of the Hydrophobic Effect. *J. Phys. Chem. B* **2002**, *106*, 521–533.